Superconducting spintronics with magnetic domain walls

Jacob Linder[1,*] and Klaus Halterman[2,*]
[1]*Department of Physics, Norwegian University of Science and Technology, N-7491 Trondheim, Norway*
[2]*Michelson Lab, Physics Division, Naval Air Warfare Center, China Lake, California 93555, USA*
(Received 15 April 2014; revised manuscript received 27 August 2014; published 8 September 2014)

The recent experimental demonstration of spin-polarized supercurrents offers a venue for establishment of a superconducting analog to conventional spintronics. Whereas domain-wall motion in purely magnetic structures is a well-studied topic, it is not clear how domain-wall dynamics may influence superconductivity and whether some functional property can be harnessed from such a scenario. Here, we demonstrate that domain walls in superconducting systems offer a unique way of controlling the quantum state of the superconductor. Considering both the diffusive and ballistic limits, we show that moving the domain wall to different locations in a Josephson junction will change the quantum ground state from being in a 0 state to a π state. Remarkably, we also show that domain-wall motion can be used to turn on and off superconductivity: the position of the domain wall determines the critical temperature T_c and thus whether the system is in a resistive state or not, causing even a quantum phase transition between the dissipationless and normal state at $T = 0$. In this way, one achieves dynamical control over the superconducting state within a single sample by utilizing magnetic domain wall motion which has interesting consequences in terms of a domain-wall-controlled superconducting magnetoresistance effect.

DOI: 10.1103/PhysRevB.90.104502 PACS number(s): 74.50.+r

I. INTRODUCTION

The research fields of spintronics and superconductivity, once disparate, have in recent years been moved closer to one another due to several key discoveries. The unification of these two fields might seem futile at first glance since ferromagnets are spin-polarized whereas the main constituent of a superconductor, the Cooper pair, resides in a spinless singlet state in conventional Bardeen-Cooper-Schrieffer theory [1]. Nevertheless, it turns out that the mutual interplay between magnetism and superconductivity opens a rich vista of new physics far beyond the notion that ferromagnetic order has a detrimental influence on superconducting order. Even setting aside for the moment the possibility of intrinsically unconventional spin-triplet superconductors such as Sr_2RuO_4 [2] and uranium-based heavy-fermion compounds [3–5] such as UGe_2, URhGe, and UCoGe, it has been realized over the last years that proximate structures of ferromagnets and perfectly conventional s-wave superconductors can sustain long-ranged and spin-polarized superconducting correlations, even in extreme environments such as half-metallic compounds [6].

The core principles which make possible such an unlikely synthesis between magnetic and superconducting order are the Pauli principle and symmetry breaking [7–9]. The former dictates that Cooper pairs in superconductors are not necessarily confined to a spinless state, but that a spin-polarized state may arise as long as the overall wave function of the pair satisfies fermionic interchange statistics. Such a change in spin polarization of the Cooper pair can be triggered by considering hybrid structures composed of ferromagnets and superconductors. Since translational symmetry is explicitly broken at the interface region, the Cooper pair wave function becomes a mixture of its original bulk state and a state with new symmetries generated at the interface region [10,11]. Cooper pairs with electrons that carry the same spin would not be subject to paramagnetic pair breaking and could in principle propagate for large distances $\sim$100 nm inside the ferromagnet regardless of the strength of the exchange field, limited only by coherence-breaking processes such as inelasticity, spin-flip scattering, and thermal decoherence.

Precisely such behavior can occur in textured ferromagnets, to be contrasted with monodomain ferromagnets. In fact, such long-ranged and spin-polarized superconducting correlations may arise even from conventional s-wave superconductors when a magnetic inhomogeneity of some sort is present [12]. A number of proposals have been put forth in this regard, ranging from multilayered magnetic structures, domain-wall ferromagnets, and interfaces with spin-active scattering [13–20] and also with a focus on the relation to magnetoresistance effects [21,22]. Moreover, the appearance of higher harmonics in the current-phase relation in SFS junctions has recently been shown to be intimately linked to the long-ranged and spin-polarized nature of such supercurrents [23–26]. Experiments have quite recently been able to unambiguously verify the existence of long-ranged supercurrents flowing through textured magnetic structures [6,27,28]. By now, it is then established that the superconducting proximity effect in ferromagnets may become long-ranged and spin-polarized under suitable circumstances. Although this is certainly interesting from a fundamental physics viewpoint, it begs the question: can these spin-polarized superconducting correlations be utilized for some practical purpose?

Spin-polarized resistive currents are known to play an instrumental role in the field of spintronics. One of their hallmarks in this context is the ability to transfer angular momentum to the magnetic order parameter in a material, an effect known as spin-transfer torque [29,30]. One of the most actively pursued research directions in this field is as of today controllable domain-wall motion, which may be accomplished via several routes [31] such as spin-polarized currents, magnons, and external magnetic fields. Now, such domain walls provide an ingredient to generate spin-polarized superconducting correlations as they represent an inhomogeneous magnetization texture. Therefore, the generation of

[*]Both authors contributed equally to this work.

spin-polarized supercurrents junctions may be used to obtain a superconducting spin-transfer torque acting on the magnetization of a ferromagnet [32–35]. Supercurrents flowing through magnetic domain walls have also been investigated experimentally [36]. In terms of domain-wall dynamics, the dissipationless nature of the supercurrent flow offers an interesting venue in terms of reduced energy loss and Joule heating, one of the main obstacles for efficient wall motion. Conversely, one should also expect a reciprocal effect, namely that the domain wall itself will influence how the triplet superconducting correlations are manifested in the system. It is this topic that we shall address in the present paper, demonstrating an intriguing outcome.

In this work, we will show that domain walls in superconducting junctions offer a way of exerting control of the quantum ground state of the system. Varying the position of a domain wall with a realistic magnetization profile taking into account magnetic anisotropy and spin stiffness, we demonstrate that the position of the domain wall controls whether the junction is in a 0 or π state. In this way, it becomes possible to exert dynamic control over the quantum ground state within a single sample: the motion of the domain wall manipulates the proximity effects responsible for the oscillatory nature of the superconducting order parameter in the ferromagnetic (F) region, as well as the magnetic correlations and destruction of superconductivity in the superconducting (S) layers. Moreover, we will show that the domain-wall dynamics can result in an effective superconducting switch, where the system changes from a resistive state to a dissipationless one. We compute the critical temperature of a domain-wall nanostructure in the ballistic regime in an entirely self-consistent manner, which is necessary when it is unknown *a priori* what the ground state of the system is. We find suitable spin-switch candidates that transition from a superconducting state to a normal one, even at $T = 0$, as the domain wall is shifted. These results show that superconducting spintronics via magnetic domain wall motion can be used not only to change the superconducting quantum state, but even turn superconductivity itself on and off (see Fig. 1). Interestingly, this also implies that a huge magnetoresistance-like effect controlled by domain-wall motion would take place in this system since it would be tuned from a dissipative to superconducting state via the domain-wall position which thus corresponds to vastly different resistances depending on the magnetization configuration of the system.

We first outline the theoretical framework used in our calculations to compute the superconducting quantum ground state. Next, we present analytical and numerical results for 0-π transitions both in the ballistic and diffusive regime of transport, including the possibility of switching from a resistive to dissipationless state simply by moving the domain wall. We then give a detailed discussion of our results, including candidate materials for the predicted effects, and experimental feasibility of our proposed setup. Finally, we summarize our findings.

II. DOMAIN WALLS IN JOSEPHSON JUNCTIONS

To model a realistic domain wall, we minimize the free energy functional for an inhomogeneous ferromagnet

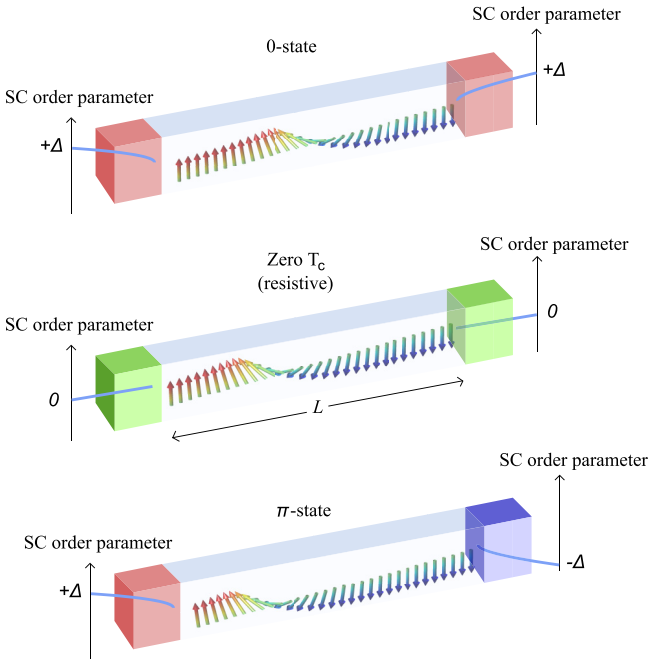

FIG. 1. (Color online) Proposed setup. A magnetic domain wall is present in a ferromagnetic layer of width L, separating two conventional s-wave superconductors. Inducing domain-wall motion to a new position can alter the quantum ground state of the junction, triggering a 0-π transition. Moving the domain-wall changes the critical temperature T_c and may even reduce it to zero (middle figure), thus destroying superconductivity. The domain-wall can be moved via an applied current, external field, or spin-wave excitations to specific locations by artificially tailored pinning sites, e.g., via geometrical notches in the sample.

including exchange stiffness and anisotropy:

$$\mathcal{F} = \int dx \left[A(\partial_x \mathbf{M})^2/2 - K_{\text{easy}} M_z^2 + K_{\text{hard}} M_x^2 \right]. \quad (1)$$

Here, A is the exchange stiffness while K_{easy} and K_{hard} are the anisotropy energies associated with the easy and hard axes of the magnetization, $\mathbf{M}$, respectively. The result [37] is $\mathbf{M}(x) = M_0[0, \sin\theta(x), \cos\theta(x)]$ where $\theta(x)$ determines the domain-wall profile and is given by

$$\theta(x) = 2\arctan\{\exp[(x - X)/\lambda]\}, \quad (2)$$

where $\lambda = \sqrt{A/K_{\text{easy}}}$ is the domain-wall width. We have also introduced the position of the center of the domain wall X, which will play an important role in what follows. With the magnetization texture in hand, we now insert it into the corresponding equations of motion for the Green's function which in turn enables us to compute the supercurrent in the system. In the diffusive regime, we make use of the quasiclassical Usadel equation [38] with the above magnetization profile $\mathbf{M}(x)$:

$$D[\hat{\partial}, \hat{G}[\hat{\partial}, \hat{G}]] + i[\varepsilon\hat{\rho}_3 + \text{diag}[\mathbf{h}\cdot\underline{\sigma}, (\mathbf{h}\cdot\underline{\sigma})^{\tau}], \hat{G}] = 0. \quad (3)$$

Here D is the diffusion constant, $\mathbf{h}||\mathbf{M}$ is the exchange field, ε is the quasiparticle energy, $\hat{\partial}$ is the derivative operator, $\hat{G}$ represents the total Green's function, and $\hat{\rho}_3$ and $\underline{\sigma}$ are 4×4 and 2×2 Pauli matrices, respectively. The Usadel equation is supplemented by the Kupriyanov-Lukichev [39] boundary

conditions at interfaces along the x axis:

$$2\zeta \hat{G}\hat{\partial}\hat{G} = \pm[\hat{G}_{\rm BCS}(\phi_\pm),\hat{G}], \tag{4}$$

in which $\hat{G}_{\rm BCS}$ is the bulk solution, $\pm$ ($\phi_\pm$) denotes the left and right interface (superconducting phase), and ζ controls the interface transparency. Note that the exchange field h also sets the length scale for the ferromagnetic coherence length $\xi_F = \sqrt{D/h}$ (and later, in the ballistic limit, $\xi_F \propto 1/h$). For stability in the numerical computations, we use the so-called Ricatti parametrization [40] of the Green's function. Finally, the supercurrent may be computed according to the formula:

$$I_{\rm super} = j_0 \int_0^\infty d\varepsilon\ {\rm Tr}\left\{\hat{\rho}_3\left(\check{g}\frac{\partial \check{g}}{\partial x}\right)^K\right\}, \tag{5}$$

where $j_0 = -N_0|e|D/16$ is a normalization constant where N_0 is the normal-state density of states and e is the electron charge. The key observation is that when the Josephson current $I_{\rm super}$ changes sign, a 0-π transition has taken place.

We now turn to the ballistic regime to investigate the transport and thermodynamic properties of SFS nanojunctions with controllable domain walls. We utilize the microscopic Bogoliubov–de Gennes (BdG) technique [41] which enables us to fully isolate the superconducting pairing correlations in the system and investigate the precise behavior of the proximity-induced supercurrent. In terms of the quasiparticle amplitudes $u_{n\sigma}$ and $v_{n\sigma}$ with excitation energy ϵ_n and spin σ, the BdG equations are compactly written as

$$\begin{pmatrix} \mathcal{H}-h_z & -h_x+ih_y & 0 & \Delta \\ -h_x-ih_y & \mathcal{H}+h_z & \Delta & 0 \\ 0 & \Delta^* & -(\mathcal{H}-h_z) & -h_x-ih_y \\ \Delta^* & 0 & -h_x+ih_y & -(\mathcal{H}+h_z) \end{pmatrix}\Psi_n = \epsilon_n\Psi_n, \tag{6}$$

where we define the vector $\Psi_n \equiv (u_{n\uparrow},u_{n\downarrow},v_{n\uparrow},v_{n\downarrow})^T$. The pair potential $\Delta(x)$ must be determined self-consistently by solving the BdG equations together with the condition

$$\Delta(x) = \frac{g(x)}{2}\sum_n [u_{n\uparrow}(x)v^*_{n\downarrow}(x) + u_{n\downarrow}(x)v^*_{n\uparrow}(x)]\tanh\left(\frac{\epsilon_n}{2T}\right), \tag{7}$$

where $g(x)$ is the attractive interaction that exists solely inside the superconducting region and restricts the sum to those quantum states with positive energies below an energy cutoff, specified below. The single-particle Hamiltonian $\mathcal{H}$ is expressed as $\mathcal{H} = 1/(2m)(-\partial_x^2 + k_x^2 + k_y^2) - \mu + U(x)$, where μ is the Fermi energy and $U(x)$ is the spin-independent interface scattering potential which we take to be of the form $U(x) = U_B[\delta(x + L/2) + \delta(x - L/2)]$, where L is the width of the ferromagnetic region. The terms $1/(2m)(k_x^2 + k_y^2)$ in the Hamiltonian represent the energy of the transverse modes.

To determine the self-consistent ground state of the SFS system, one must calculate the free energy, $\mathcal{F}$, given by

$$\mathcal{F} = -2T\sum_n \ln\left[2\cosh\left(\frac{\epsilon_n}{2T}\right)\right] + \frac{\langle|\Delta(x)|^2\rangle}{g}, \tag{8}$$

where $\langle\ldots\rangle$ denotes spatially averaging over the entire system, and the pair potential is self-consistently calculated in Eq. (7). The supercurrent can be found by taking the derivative of the free energy with respect to the phase difference ϕ: $j_x = 2e(\partial\mathcal{F}/\partial\phi)$. Note that we have not made any assumption of a weak proximity effect in the above; the results are obtained by solving the full proximity effect equations numerically. We normalize the energy scales by the zero-temperature bulk superconducting gap, Δ.

III. INDUCING A 0-π TRANSITION VIA DOMAIN-WALL MOTION

We start by demonstrating the possibility of having 0-π transitions induced by moving the domain wall in the diffusive regime. In Figs. 2(a)–2(b) and 2(c)–2(d) we have computed the supercurrent-phase relation and critical current using two different parameter sets for the sake of showing that this effect does not just occur for special fine-tuned parameters. Figures 2(b) and 2(d) illustrate the critical current as a function of the domain-wall position X in the ferromagnet. In all plots, the transition is clearly seen: the current-phase relation is inverted whereas the critical current decays towards zero and then rises to finite values. The usage of the quasiclassical Usadel equation places a limitation on how strong exchange fields h that we may consider. Nonetheless, Fig. 2 shows that the domain-wall position continues to induce 0-π transitions when raising the exchange field and there is no reason to expect different behavior for even stronger ferromagnets where the exchange field constitutes a considerable fraction of the Fermi energy.

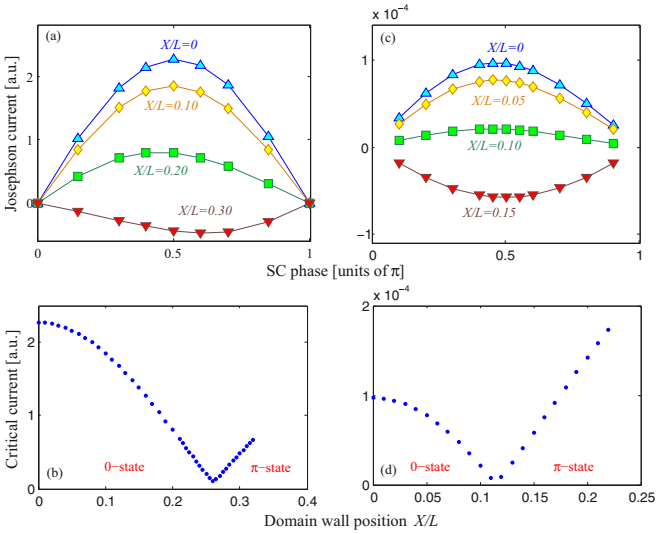

FIG. 2. (Color online) Josephson current in the diffusive limit. Supercurrent-phase relation and critical current for two different parameter sets. (a), (b): $h/\Delta = 8, \lambda/L = 0.05, L/\xi = 1.5$; (c), (d): $h/\Delta = 30$, $\lambda/L = 0.1$, $L/\xi = 1$. In all cases, we have used an interface parameter $\zeta = 4$, corresponding to a weakly transparent interface in terms of tunneling, and a temperature $T/T_c = 0.1$. To make contact with the experimental setting, we note that weak exchange fields of order a few Δ (corresponding to ~5 meV) have been reported in weak PdNi ferromagnetic alloys [42]. We also underline that ξ above is the bulk superconducting coherence length, which can exceed 100 nm in dirty bulk superconductors such as Al. The parameter sets used above are thus accessible experimentally.

In fact, one should expect to see 0-π oscillations induced by even smaller increments of the domain-wall position, precisely as seen when comparing Figs. 2(b) and 2(d). We note that our calculation is done for a scenario where the system has relaxed to equilibrium with the domain wall at position X in the junction, thus corresponding to several measurements of the current (yet within one single sample) with the domain wall at rest in different positions. We will later discuss precisely how this may be accomplished experimentally. An alternative measuring scheme would consist of doing measurements on distinct samples with domain walls at pinned, predetermined locations by means of geometrical notches or other sources of pinning potentials in the ferromagnet [43].

The underlying physics for this phenomenon may be most easily understood in the limit of a infinitesimally thin domain wall. In that case, one may think of the ferromagnetic region as an effective bilayer with two ferromagnets in an antiparallel configuration. Whether the junction is in a 0 or π state is determined by the total phase shift picked up by an Andreev bound state carrying the supercurrent through the ferromagnet. This phase shift depends on the exchange field orientation and the length of the junction. When the ferromagnet consists of two regions with antiparallel magnetization, the phase shift is partially compensated when the bound state first propagates through one ferromagnet and then the second one with opposite magnetization direction. In fact, when the layers have exactly the same width, the junction is essentially equivalent to an SNS system [44]. However, if the layers are allowed to have different thicknesses, the phase shift picked up by the Andreev bound state will allow for a π state to be formed as long as h and/or L are sufficiently large to induce a π-phase difference as the bound state makes a full round trip between the superconductors. We can then qualitatively understand why moving the domain wall will induce 0-π transitions: the position of the wall determines the effective phase shift experienced by the Andreev bound state as it propagates between the superconductors. When the domain wall is finite, the analogy to a bilayer breaks down since spin rotation takes place and induces a strong magnetization component perpendicular to the easy axis close to the domain-wall center. In our approach, we have access to an arbitrary domain-wall profile and have verified that the domain-wall position still determines whether the junction is in a 0 or π state in the case where the domain wall extends over a large part of the junction. We demonstrate this in Fig. 3 for several choices of the domain-wall width λ. The curves in the panels correspond to different domain-wall positions X such that the entire domain wall always fits inside the junction—in this way, we make certain to probe only the effect of the position of the domain wall rather than to produce a qualitatively different shape of the magnetization texture. The blue curves represent a 0 state whereas the orange curves denote a π state. When the domain-wall width λ increases sufficiently, the transition between these quantum states is lost. Interestingly, the position X of the domain wall where the transition occurs depends in a nonmonotonic fashion on the width λ. This is ultimately a reflection of the oscillatory dependence on the spin-dependent phase shifts accumulated by quasiparticles traveling through the ferromagnetic region, with the phase shifts depending on both the position X and the width λ. We emphasize here

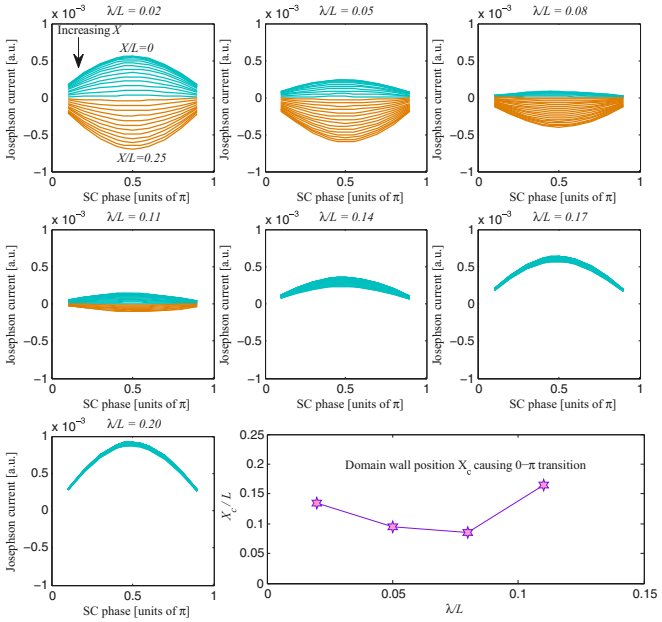

FIG. 3. (Color online) Role of domain-wall width for 0-π transitions. Supercurrent-phase relation for the case $h/\Delta = 30$ and $L/\xi = 1$, using a weakly transparent interface $\zeta = 4$ with a temperature $T/T_c = 0.1$. Various domain-wall widths λ are considered and the curves in each panel represent the position X of the domain-wall center ranging from the middle of the junction $X/L = 0.0$ to $X/L = 0.25$. In this way, the entire domain wall always fits inside the junction. We also plot the position X_c where the junction makes a transition from a 0 to a π state as a function of λ.

that even for domain walls with $\lambda/L \ll 1$, the actual extension of the domain wall determined by the profile Eq. (2) covers a considerable portion of the junction and does not correspond to an abrupt bilayer setup (see Appendix and Fig. 7).

For the ballistic results, in all cases we have assumed a superconducting correlation length corresponding to $k_F\xi = 100$ and measure all temperatures in units of T_{c0}, the transition temperature of bulk S material. We consider $T = 0.01$, except when calculating the critical temperature, and fix the energy cutoff at 0.04, in units of μ. Scattering at the interfaces is characterized by parameter $Z_B \equiv mU_B/k_F$. Except when considering transition temperatures, we set $Z_B = 1$ throughout the calculations, corresponding to a moderately transparent interface in terms of tunneling. We have found however that the domain wall position leading to the 0-π transition is weakly dependent on Z_B. This follows from the fact that the magnitude of the exchange interaction h shifts the energy spectrum for spin-up and spin-down quasiparticles by an amount $-h$ and $+h$, respectively. Thus, the oscillatory period of the superconducting correlations in F are primarily determined from the difference of the spin-up and spin-down wave vectors, and not the spin-independent interface scattering.

In the ballistic regime, Fig. 4 demonstrates the thermodynamics of the 0-π transition, which follows from the free energy. We characterize the ground state by finding $\mathcal{F}_S$, the free energy of the whole system in the self-consistent state, and $\mathcal{F}_N$, the normal-state ($\Delta \equiv 0$) free energy. The normalized condensation free energy is then $\Delta\mathcal{F} \equiv (\mathcal{F}_S - \mathcal{F}_N)/(2E_0)$,

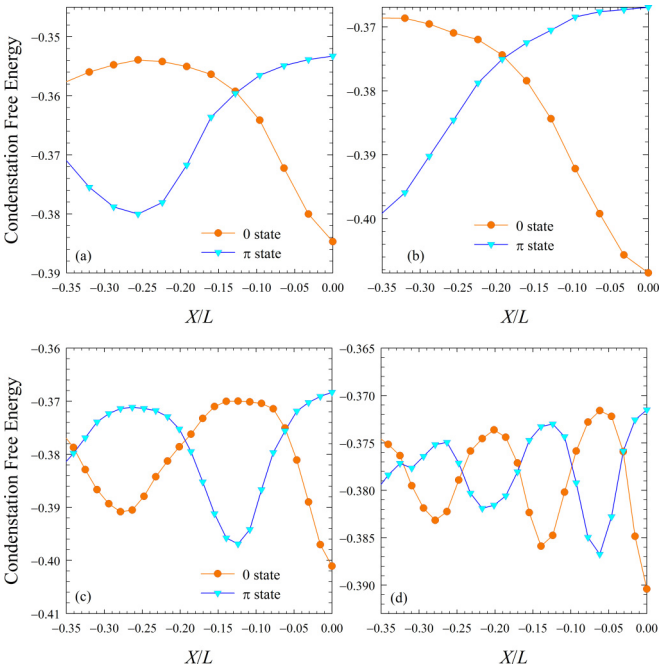

FIG. 4. (Color online) Free energy in the ballistic limit. Control of the quantum state with domain wall motion: (a) depicts the condensation free energy as a function of domain wall motion for both of the self-consistently determined π and 0 states. Here $\lambda/L = 0.02$, $L/\xi = 1.5$, and $h/\Delta = 5$. (b) corresponds to $L/\xi = 1$ with all other parameters the same as (a). The center of the junctions corresponds to $X/L = 0$. The effects of larger exchange fields for $L/\xi = 1$ are shown in (c) and (d) where $h/\Delta = 5\pi$ and 10π, respectively.

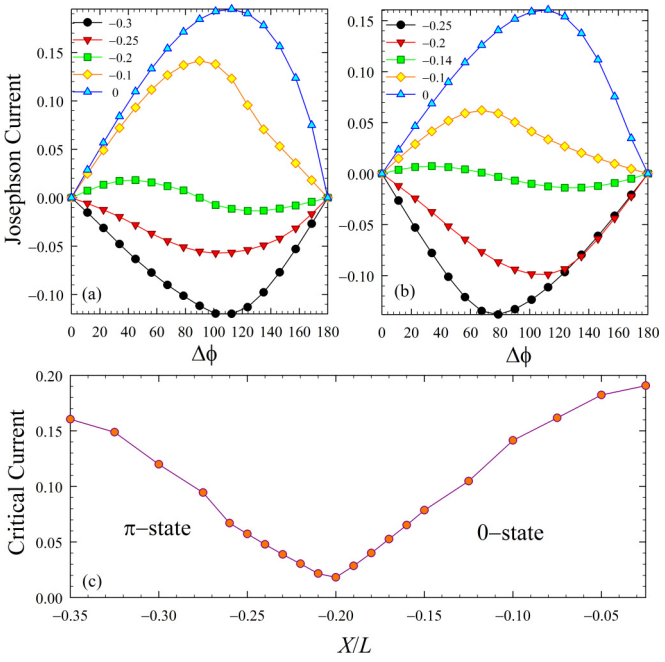

FIG. 5. (Color online) Josephson current in the ballistic limit. Supercurrent-phase relation for two different ferromagnet widths: (a) $h/\Delta = 5, \lambda/L = 0.02, L/\xi = 1$ and (b) $L/\xi = 1.5$. In both cases there is a clear appearance of a second harmonic in the Josephson relation near the 0-π transition. (c) Critical supercurrent as a function of domain-wall position for the same F thickness used in (a).

where E_0 is the condensation energy of bulk S material at $T = 0$. By comparing the condensation energies of the 0 and π state configurations as a function of the domain-wall position, we can therefore immediately identify the ground state of the system. For both Figs. 4(a) and 4(b), we see that when the domain wall is located near the center of the ferromagnet ($X = 0$), the 0 state is the ground state. However, when the domain wall is moved closer to the interface, the ground state is the π state. Since the singlet pair correlations in the magnet oscillate with a period that is inversely proportional to h, it is expected that larger exchange fields should result in greater possibilities for π ground states when varying the domain-wall position. In Figs. 4(c) and 4(d), we see the periodicity in the free energy as a function of X whose oscillations clearly double when doubling h, and indeed many more 0-π state transitions are observed.

Next, in Fig. 5 we examine the charge transport and calculate the Josephson current for the same thicknesses in Figs. 4(a) and 4(b). Additional details of the numerical procedure are given in the Appendix. The free energy profiles in Fig. 4 revealed that the 0-π crossover occurs at $X/L \approx -0.14$ and $X/L \approx -0.2$ for $L = 1.5\xi$ and $L = \xi$, respectively. This is consistent with the supercurrent behavior of Fig. 5, where for those domain-wall positions, the current-phase relation acquires additional harmonics at the 0-π transition. An experimentally relevant quantity related to the above results is the critical current. We therefore show in Fig. 5(c) the critical current as a function of domain-wall position for the cases considered in (a). This quantity is determined by finding the maximum value of the magnitude of the Josephson current over the entire $\Delta\phi$ interval, for each X. The critical current then has a minimum at the 0-π transition corresponding to the cusp at $X/L \approx -0.2$. Note that the observed behavior is robust in the sense that it is found in both the ballistic and diffusive limit, and for differing thicknesses. This should facilitate making contact with experiment.

IV. SUPERCONDUCTING ON-OFF SWITCH VIA DOMAIN-WALL MOTION

We next demonstrate that one can obtain a superconducting switch controlled by the position of the domain wall. This effect is revealed in the experimentally relevant critical temperature, which is computed by treating $\Delta(x)$ as a small parameter and linearizing the BdG equations, Eq. (6). Controlling T_c requires the structure to be finite sized, and hence for configurations leading to switching effects, we adopt hard-wall boundary conditions at the outer edges. Near the transition, we can thus write [45] $\Delta_i = \sum_q J_{iq}\Delta_q$, where Δ_i are the expansion coefficients with respect to a standing wave basis, $\phi_i = \sqrt{2/d}\sin(i\pi x/d)$, and $J_{iq} \equiv (J^u_{iq} + J^v_{iq})/2$, where,

$$J^u_{iq} = \Gamma \int d\epsilon_\perp \sum_n \left[\tanh\left(\frac{\epsilon^{u,0}_n}{2T}\right) \sum_m \frac{F^*_{qnm} F_{inm}}{\epsilon^{u,0}_n - \epsilon^{v,0}_m} \right], \quad (9)$$

$$J^v_{iq} = \Gamma \int d\epsilon_\perp \sum_n \left[\tanh\left(\frac{\epsilon^{v,0}_n}{2T}\right) \sum_m \frac{G_{qnm} G^*_{inm}}{\epsilon^{v,0}_n - \epsilon^{u,0}_m} \right]. \quad (10)$$

Here, $\Gamma = \gamma/(4\pi k_F d)$, with γ equal to the dimensionless coupling constant in S, and d is the total width of the system. The integral over $\epsilon_\perp$ accounts for the transverse in-plane quasiparticle energies. We also define $F_{inm} = \pi\sqrt{2d}\sum_{pq}(u^0_{np\uparrow}u^0_{mq\downarrow} + u^0_{np\downarrow}u^0_{mq\uparrow})K_{inm}$, $G_{inm} = \pi\sqrt{2d}\sum_{pq}(v^0_{np\uparrow}v^0_{mq\downarrow} + v^0_{np\downarrow}v^0_{mq\uparrow})K_{inm}$, where $K_{inm} \equiv \int_0^d dx g(x)\phi_i(x)\phi_n(x)\phi_m(x)$. The u^0_{np} and v^0_{mq} are the expansion coefficients of the unperturbed $[\Delta(x) = 0]$ quasiparticle amplitudes in terms of the basis set. Similarly, $\epsilon^{u,0}_n$ and $\epsilon^{v,0}_n$ are the unperturbed quasiparticle energies. Penetration of the superconducting condensate into the ferromagnet results in the breaking of Cooper pairs by the exchange field and leads to a decrease of the superconducting transition temperature. The transition T_c is the critical temperature at which the S regions become normal so that $\Delta(x) = 0$ is the only solution of the self-consistency equation. By varying the temperature and finding the corresponding eigenvalues of the matrix, J_{iq}, it is straightforward to extract T_c [45].

We illustrate in Fig. 6(a) the rich variety of switching behavior that can arise when varying the domain-wall position. We consider superconducting leads with widths on the order of ξ. Increasing the exchange field tends to increase the number of T_c oscillations, reflecting the increase in the period of oscillations in the Cooper pairing amplitude that resides in the ferromagnet. The critical temperature is typically indifferent to h near the center of the junction, where the curves coalesce. As the domain wall shifts away from the center, T_c of the system drops abruptly to zero and the system transitions to a normal resistive state in a way that depends strongly on h. This is highly suggestive of a superconducting switch where superconductivity is turned off or on depending on the location of the domain wall. The application of an external field may also introduce additional interesting reentrance effects [46]. It is important to note that this switching effect is not exclusive to Josephson junctions, as we have found that the same effect occurs in a S/F bilayer structure as well. We illustrate this point in Fig. 6(b), where the critical temperature vs domain-wall position is shown for a bilayer with the same exchange fields in panel (a). We again observe similar switching effects that were found in the Josephson junction configuration, thus demonstrating the robustness of this phenomena. The critical temperature for bilayers in the dirty limit was found to be reentrant for a different type of domain structure [47] that exhibits magnetization rotation across the F layer (rather than through it). In that case, there are no long-range triplet correlations present. The critical temperature in SFF systems where the magnetization is uniform in each F layer can also exhibit spin valve effects [48–50]; however for collinear magnetization states, only the singlet and opposite-spin triplet correlations can be induced.

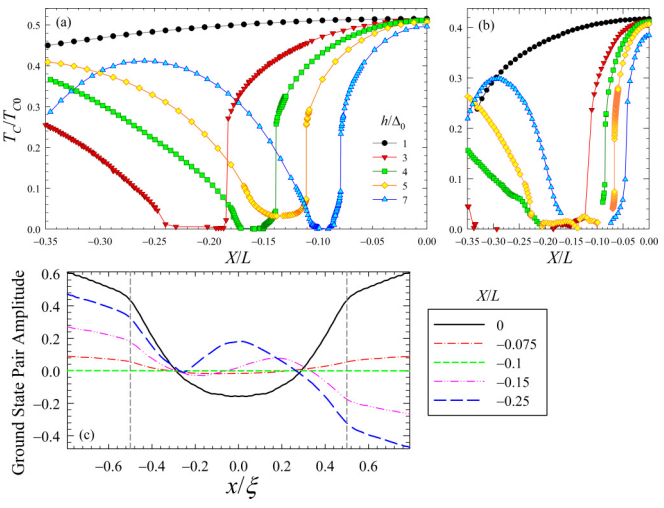

FIG. 6. (Color online) Controlling T_c with domain-wall motion. (a) Turning superconductivity on or off: Critical temperature for a SFS junction as a function of domain-wall position for several different exchange fields (see legend). We assume here that $\lambda/L = 0.02$, $d_S = 0.95\xi$, $L/\xi = 1$, and $Z_B = 0$. (b) Critical temperature vs domain-wall position for a S/F bilayer. We consider the same parameter values that were used in (a) except the superconductor width corresponds to $d_S = \xi$. In (c) we show the Cooper pair amplitude for the SFS ground states when $T = 0$ and for an exchange field of $h/\Delta = 7$. Its spatial dependence reveals the transition from the π to 0 state near the minimum of the T_c curve in (a) occurring at $X/L \approx -0.1$, where the system has transitioned to a normal resistive state. Vertical dashed lines denote the interfaces between the S and F regions.

In analogy with the critical current behavior, the critical temperature contains fingerprints of the 0-π transition, occurring at around the minimum of the T_c curves. This point is illustrated in Fig. 6(c), where we show the spatial behavior of the Cooper pair amplitude for an SFS junction [case (a)] and $h/\Delta = 7$. Five differing domain-wall positions are considered: two above and two below $X/L \approx -0.1$, where the entire SFS system is normal and the pair amplitude vanishes. Clearly, the domain-wall position relative to this transition point dictates whether the ground state of the system is the 0 or π state.

V. IMPLICATIONS FOR EXPERIMENTS

It is known [31] that domain-wall motion may be induced both via application of a current-induced spin-transfer torque and via external magnetic fields [51]. Besides these conventional techniques, another possibility was recently unveiled which might be suitable for our purposes. It was demonstrated in Ref. [52] that domain-wall motion could be obtained via excitation of spin waves, resulting in a purely magnonic spin-transfer torque. Such spin waves could be excited via application of a local ac magnetic field $\mathbf{H} = H_0 \sin(\omega t)\hat{z}$, giving rise to domain-wall motion toward the spin-wave source. Application of such local fields has been successfully implemented experimentally previously [53], and might be feasible in our setup as well. Current-induced domain-wall motion is also an alternative, although it might require an additional polarizing ferromagnetic layer in order to achieve an efficient spin-transfer torque. It has been demonstrated that spin-triplet correlations can induce magnetization dynamics and spin-transfer torques [32–35,54], and it is thus reasonable to expect that domain-wall motion in a Josephson junction can be induced by a supercurrent spin-transfer torque as well. It should be noted that the required current densities to move domain walls are of order 10^4–10^5 A/cm^2, values which have been obtained for the critical current density in SFS junctions [55]. Once domain-wall motion has been induced via, e.g., one of the above mentioned venues, it is possible to control

where the motion terminates, and thus obtain a new ground-state configuration, by artificially tailoring pinning sites which effectively traps the domain wall. This can be accomplished experimentally by, e.g., making geometrical notches at the desired locations of the ferromagnetic film/wire [43]. Based on the above discussion, there should then be several alternatives available experimentally in order to move the domain wall in the proposed Josephson junction and thus tune the quantum state of the system to either a 0 or π junction and even turn superconductivity on and off. In terms of candidate materials for observation of the predicted effects, one would need two standard s-wave superconductors, such as Nb or Al, and a magnetic region supporting a domain wall with a width of order 5–10 nm. Such domain walls are known to occur in thin magnetic films Pt/Co/AlO$_x$, PtI(Co/Pt)$_n$, and (Co/Ni)$_n$ (see, e.g., Ref. [56] for a review). It could also possible to use standard ferromagnets such as Fe, Co, Ni, and their alloys that typically feature domain walls which are several tens and up to a hundred nanometers, but where the wall thickness can be strongly reduced down to $\sim$10 nm by reinforcing shape anisotropy in magnetic nanowires [57]. Moreover, although we have in our work considered a Bloch-type of domain wall, we do not expect any qualitative change for Neel or head-to-head domain walls, whose textures may be obtained by a rotation in spin space, since the physical principle remains the same. This is advantageous in the sense that generic domain walls, as opposed to a specific type of wall texture, will suffice to experimentally observe the influence on superconductivity predicted here. Finally, we note that the domain-wall profile can be altered from the 180° Walker profile considered here in certain experimental systems such as nanopillars where a more complicated domain wall structure may arise. The effect of multiple pinned domains at various locations in the ferromagnet is an interesting future prospect to consider.

VI. CONCLUSION

We have shown that domain wall motion in superconducting junctions provides a unique way to both tune the quantum ground state between 0 and π phases and also turn on and off superconductivity itself. In particular, we find that the domain-wall motion may even trigger a quantum phase transition between a resistive and dissipationless state. Our results point towards new ways to merge superconductivity and spintronics in order to achieve functional properties by utilizing domain-wall motion.

ACKNOWLEDGMENTS

J.L. was supported by the Research Council of Norway, Grant No. 205591/F20 (FRINAT). K.H. was supported in part by a grant of HPC resources and the ILIR program sponsored by ONR.

APPENDIX A: NUMERICAL METHOD FOR THE BALLISTIC REGIME

We here provide additional details regarding the self-consistent calculation of the Josephson current in the ballistic limit. It is convenient numerically to determine the Josephson current using the previously calculated quasiparticle amplitudes and energies. Before presenting our method for computation of the supercurrent, we first discuss here the charge conservation laws. From the Heisenberg equation,

$$\frac{\partial}{\partial t}\langle\rho(\mathbf{r})\rangle = i\langle[\mathcal{H}_{\rm eff},\rho(\mathbf{r})]\rangle, \tag{A1}$$

where the effective Hamiltonian $\mathcal{H}_{\rm eff}$ that we use to model our SFS system takes the form

$$\begin{aligned}\mathcal{H}_{\rm eff} = \int d^3r\Bigg\{&\sum_\alpha \psi_\alpha^\dagger(\mathbf{r})\Big(-\frac{\nabla^2}{2m}-\mu\Big)\psi_\alpha(\mathbf{r})\\ &+\frac{1}{2}\Bigg[\sum_{\alpha,\beta}(i\sigma_y)_{\alpha\beta}\Delta(\mathbf{r})\psi_\alpha^\dagger(\mathbf{r})\psi_\beta^\dagger(\mathbf{r})+\text{H.c.}\Bigg]\\ &-\sum_{\alpha,\beta}\psi_\alpha^\dagger(\mathbf{r})(\mathbf{h}\cdot\boldsymbol{\sigma})\psi_\beta(\mathbf{r})\Bigg\},\end{aligned} \tag{A2}$$

where $\psi_\alpha^\dagger$ and ψ_α are the usual creation and annihilation operators with spin α, respectively, and $\boldsymbol{\sigma}$ are the Pauli matrices. Performing the above commutator yields the continuity condition,

$$\frac{\partial}{\partial t}\langle\rho(\mathbf{r})\rangle + \nabla\cdot\mathbf{j} = -4e\text{Im}[\Delta(\mathbf{r})\langle\psi_\uparrow^\dagger(\mathbf{r})\psi_\downarrow^\dagger(\mathbf{r})\rangle]. \tag{A3}$$

In the steady state considered here, the first term on the left is absent. Thus, for our quasi-one-dimensional geometry, the conservation law can be rewritten as

$$\frac{\partial j_y(x)}{\partial x} = 2e\text{Im}\left\{\Delta(x)\sum_n[u_{n\uparrow}^* v_{n\downarrow}+u_{n\downarrow}^* v_{n\uparrow}]\tanh\left(\frac{\epsilon_n}{2T}\right)\right\}. \tag{A4}$$

When the pair potential is self-consistently determined using Eq. (7), the right-hand side of Eq. (A4) vanishes, yielding a constant current. If the self-consistency condition is not strictly satisfied, the terms on the right act effectively as sources of current.

Starting with the quantum mechanical expectation value of the momentum density, we can can express the quasiparticle current density j_x in terms of the quasiparticle amplitudes as

$$j_x = -\frac{e}{2m}\sum_{n,\sigma}\left\langle -i\psi_\sigma^\dagger\frac{\partial}{\partial x}\psi_\sigma + i\left(\frac{\partial}{\partial x}\psi_\sigma^\dagger\right)\psi_\sigma\right\rangle \tag{A5}$$

$$= \frac{2e}{m}\text{Im}\left\{\sum_{n,\sigma}\left[u_{n\sigma}\frac{\partial u_{n\sigma}^*}{\partial x}f_n + v_{n\sigma}\frac{\partial v_{n\sigma}^*}{\partial x}(1-f_n)\right]\right\}, \tag{A6}$$

where f_n is the Fermi function, $f_n = 1/\{\exp[\epsilon_n/(2T)]+1\}$, and the σ can be either be either spin-up or spin-down ($\uparrow$ or $\downarrow$) relative to the z-quantization axis.

Our numerical procedure for calculating the supercurrent involves first assuming a piecewise constant form for the

pair potential in each S layer. We then discretize the spatial coordinate x_j: $x_j = (j-1)\Delta x$, where $\Delta x \equiv d/(N-1)$ for N grid points subdividing the system width d. We take d to be large enough until the results become independent of d. The next step involves Fourier-transforming the real-space BdG equations [Eq. (6)]. The quasiparticle amplitudes, Ψ_n, are thus written

$$\Psi_n(x) = \frac{1}{\sqrt{d}} \int_{-K}^{K} e^{ik_x x} \hat{\Psi}_n(k_x) dk_x, \tag{A7}$$

where $K \equiv \pi/\Delta x$. For numerical purposes, the Fourier integral is converted to a discrete sum:

$$\Psi_n(x) = \frac{1}{\sqrt{d}} \sum_{q=1}^{N} e^{ik_q x} \hat{\Psi}_q. \tag{A8}$$

We write the wave vector index as $k_q = -K + 2(q-1)K/(N-1)$, so that $\Delta k_q \equiv k_{q+1} - k_q = 2\pi/d$, corresponding to periodic boundary conditions. We can now Fourier-transform the real-space BdG equations, resulting in the following set of coupled equations in momentum space:

$$\begin{pmatrix} \hat{H}_0 - \hat{h}_z & -\hat{h}_x + i\hat{h}_y & 0 & \hat{\Delta} \\ -\hat{h}_x - i\hat{h}_y & \hat{H}_0 + h_z & \hat{\Delta} & 0 \\ 0 & \hat{\Delta}^* & -(\hat{H}_0 - \hat{h}_z) & -\hat{h}_x - i\hat{h}_y \\ \hat{\Delta}^* & 0 & -\hat{h}_x + i\hat{h}_y & -(\hat{H}_0 + \hat{h}_z) \end{pmatrix} \times \Psi_k = \epsilon_n \Psi_k, \tag{A9}$$

with matrix elements

$$\hat{H}_0(q,q') = \frac{1}{d} \int_0^d dx \left(\frac{k_q^2}{2m} + \epsilon_\perp - \mu \right) e^{i(k_q - k_{q'})x}, \tag{A10}$$

$$\hat{\Delta}(q,q') = \frac{1}{d} \int_0^d dx \Delta(x) e^{i(k_q - k_{q'})x}, \tag{A11}$$

$$\hat{h}_i(q,q') = \frac{1}{d} \int_0^d dx\, h_i(x) e^{i(k_q - k_{q'})x}, \quad i = x,y,z. \tag{A12}$$

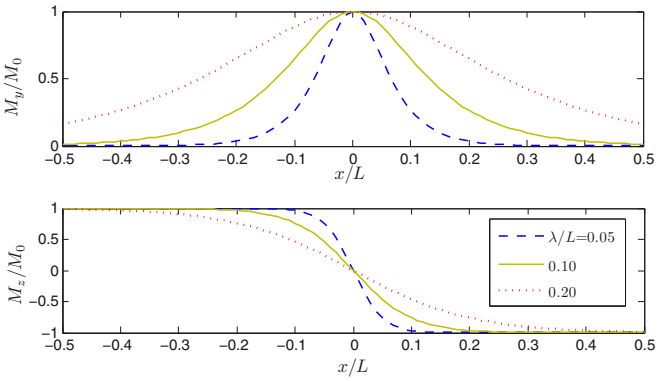

FIG. 7. (Color online) Spin-texture inside the ferromagnet. Plot of the magnetization components of the domain wall for different choices of the domain-wall width λ relative to the junction length L.

Once the momentum space wave functions and energies are found, they are transformed back into real space and the pair potential is self-consistently determined via (7). The newly calculated $\Delta(x)$ is then inserted back into the BdG equations and the above process is repeated. The requirement of self-consistency is evident in the large number of iterations generally needed to satisfy charge conservation.

We generally solve $\Delta(x)$ self-consistently within about one coherence length of each side of the domain wall/superconductor interface. This leads to the necessary constant current within that region. Deeper within the S regions, we impose that $\Delta(x)$ equals $|\Delta(x)|e^{i\phi_L}$, and $|\Delta(x)|e^{i\phi_R}$ in the left (L) and right (R) superconductor regions respectively. The corresponding phase difference $\Delta\phi = \phi_R - \phi_L$ across the S banks provides a well-defined source of current, and acts effectively as a boundary condition.

APPENDIX B: DOMAIN-WALL PROFILE

We include here for completeness a plot (Fig. 7) of the spin-texture inside the ferromagnet for different choices of the domain-wall width λ relative the junction length. As seen, the net domain-wall rotation makes this model distinct from an abrupt bilayer setup even when $\lambda \ll L$.

[1] J. Bardeen, L. N. Cooper, and J. R. Schrieffer, Phys. Rev. **106**, 162 (1957).
[2] K. D. Nelson, Z. Q. Mao, Y. Maeno, and Y. Liu, Science **306**, 1151 (2004).
[3] S. S. Saxena, Nature (London) **406**, 587 (2000).
[4] D. Aoki, A. Huxley, E. Ressouche, D. Braithwaite, J. Flouquet, J.-P. Brison, El. Lhotel, and C. Paulsen, Nature (London) **413**, 613 (2001).
[5] N. T. Huy, A. Gasparini, P. E. de Nijs, Y. Huang, J. C. P. Klaasse, T. Gortenmulder, A. de Visser, A. Hamann, T. Gorlach, and H. v. Lohneysen, Phys. Rev. Lett. **99**, 067006 (2007).
[6] R. S. Keizer, S. T. B. Goennenwein, T. M. Klapwijk, G. Miao, G. Xiao, and A. Gupta, Nature (London) **439**, 825 (2006).
[7] A. I. Buzdin, Rev. Mod. Phys. **77**, 935 (2005).
[8] F. S. Bergeret, A. F. Volkov, and K. B. Efetov, Rev. Mod. Phys. **77**, 1321 (2005).
[9] M. Eschrig and T. Löfwander, Nat. Phys. **4**, 138 (2008).
[10] Y. Tanaka, A. A. Golubov, S. Kashiwaya, and M. Ueda, Phys. Rev. Lett. **99**, 037005 (2007).
[11] M. Eschrig, T. Löfwander, T. Champel, J. C. Cuevas, J. Kopu, and G. Schön, J. Low Temp. Phys. **147**, 457 (2007).
[12] F. S. Bergeret, A. F. Volkov, and K. B. Efetov, Phys. Rev. Lett. **86**, 4096 (2001).
[13] M. Eschrig, J. Kopu, J. C. Cuevas, and G. Schön, Phys. Rev. Lett. **90**, 137003 (2003).
[14] Z. Pajović, M. Božović, Z. Radović, J. Cayssol, and A. Buzdin, Phys. Rev. B **74**, 184509 (2006).
[15] A. F. Volkov, Y. V. Fominov, and K. B. Efetov, Phys. Rev. B **72**, 184504 (2005).

[16] J. Linder, T. Yokoyama, and A. Sudbø, Phys. Rev. B **79**, 054523 (2009).
[17] K. Halterman, P. H. Barsic, and O. T. Valls, Phys. Rev. Lett. **99**, 127002 (2007).
[18] Z. Shomali, M. Zareyan, and W. Belzig, New J. Phys. **13**, 083033 (2011).
[19] T. E. Baker, A. Richie-Halford, and A. Bill, arXiv:1310.6580.
[20] A. S. Melnikov, A. V. Samokhvalov, S. M. Kuznetsova, and A. I. Buzdin, Phys. Rev. Lett. **109**, 237006 (2012).
[21] G. X. Miao, M. D. Mascaro, C. H. Nam, C. A. Ross, J. S. Moodera, Appl. Phys. Lett. **99**, 032501 (2011).
[22] B. Li, N. Roschewsky, B. A. Assaf, M. Eich, M. Epstein-Martin, D. Heiman, M. Munzenberg, and J. S. Moodera, Phys. Rev. Lett. **110**, 097001 (2013).
[23] A. I. Buzdin, Phys. Rev. B **72**, 100501(R) (2005).
[24] C. Richard, M. Houzet, and J. S. Meyer, Phys. Rev. Lett. **110**, 217004 (2013).
[25] L. Trifunovic, Phys. Rev. Lett. **107**, 047001 (2011).
[26] A. Pal, Z. H. Barber, J. W. A. Robinson, and M. G. Blamire, Nat. Commun. **5**, 3340 (2014).
[27] M. S. Anwar, F. Czeschka, M. Hesselberth, M. Porcu, and J. Aarts, Phys. Rev. B **82**, 100501(R) (2010).
[28] J. W. A. Robinson, J. D. S. Witt, and M. G. Blamire, Science **329**, 59 (2010).
[29] J. C. Slonczewski, J. Magn. Magn. Mater. **159**, L1 (1996).
[30] L. Berger, Phys. Rev. B **54**, 9353 (1996).
[31] J. Grollier, A. Chanthbouala, R. Matsumoto, A. Anane, V. Cros, F. Nguyen van Dau, and A. Fert, C. R. Phys. **12**, 309 (2011).
[32] X. Waintal and P. W. Brouwer, Phys. Rev. B **65**, 054407 (2002).
[33] E. Zhao and J. A. Sauls, Phys. Rev. B **78**, 174511 (2008).
[34] J. Linder and T. Yokoyama, Phys. Rev. B **83**, 012501 (2011).
[35] P. D. Sacramento, L. C. Fernandes Silva, G. S. Nunes, M. A. N. Araújo, and V. R. Vieira, Phys. Rev. B **83**, 054403 (2011); P. D. Sacramento and M. A. N. Araujo, Eur. Phys. J. B **76**, 251 (2010).
[36] J. W. A. Robinson, F. Chiodi, G. B. Halasz, M. Egilmez, and M. G. Blamire, Sci. Rep. **2**, 699 (2012).
[37] N. L. Schryer and L. R. Walker, J. Appl. Phys. **45**, 5406 (1974).
[38] K. Usadel, Phys. Rev. Lett. **25**, 507 (1970).
[39] M. Y. Kuprianov and V. F. Lukichev, Sov. Phys. JETP **67**, 1163 (1988).
[40] N. Schopohl and K. Maki, Phys. Rev. B **52**, 490 (1995).
[41] P. G. de Gennes, *Superconductivity of Metals and Alloys* (Addison-Wesley, Reading, MA, 1989).
[42] T. Kontos, M. Aprili, J. Lesueur, X. Grison, and L. Dumoulin, Phys. Rev. Lett. **93**, 137001 (2004).
[43] A. Himeno, T. Ono, S. Nasu, K. Shigeto, K. Mibu, and T. Shinjo, J. Appl. Phys. **93**, 8430 (2003).
[44] Y. M. Blanter and F. W. J. Hekking, Phys. Rev. B **69**, 024525 (2004).
[45] J. Zhu, I. N. Krivorotov, K. Halterman, and O. T. Valls, Phys. Rev. Lett. **105**, 207002 (2010).
[46] Z. Yang, M. Lange, A. Volodin, R. Szymczak, and V. V. Moshchalkov, Nat. Mater. **3**, 793 (2004).
[47] T. Champel and M. Eschrig, Phys. Rev. B **71**, 220506 (2005).
[48] Sangjun Oh, D. Youm, and M. R. Beasley, Appl. Phys. Lett. **71**, 2376 (1997).
[49] P. V. Leksin, N. N. Garif'yanov, I. A. Garifullin, J. Schumann, H. Vinzelberg, V. Kataev, R. Klingeler, O. G. Schmidt, and B. Büchner, Appl. Phys. Lett. **97**, 102505 (2010).
[50] C.-T. Wu, O. T. Valls, and K. Halterman, Phys. Rev. B **86**, 014523 (2012).
[51] L. Y. Zhu, T. Y. Chen, and C. L. Chien, Phys. Rev. Lett. **101**, 017004 (2008).
[52] P. Yan, X. S. Wang, and X. R. Wang, Phys. Rev. Lett. **107**, 177207 (2011).
[53] H. K. Kim, S. H. Hong, B. C. Kim, J. S. Hwang, S. M. Seong, T. H. Park, S. W. Hwang, and D. Ahn, Jpn. J. Appl. Phys. **43**, 2054 (2004).
[54] I. Kulagina and J. Linder, Phys. Rev. B **90**, 054504 (2014).
[55] V. A. Oboznov, V. V. Bol'ginov, A. K. Feofanov, V. V. Ryazanov, and A. I. Buzdin, Phys. Rev. Lett. **96**, 197003 (2006).
[56] O. Boulle, G. Malinowski, and M. Kläui, Mater. Sci. Eng., R **72**, 159 (2011).
[57] U. Ebels, A. Radulescu, Y. Henry, L. Piraux, and K. Ounadjela, Phys. Rev. Lett. **84**, 983 (2000).